Ultrafast metal-insulator-multi-wall carbon nanotube tunneling diode employing asymmetrical structure effect

Jeong Hee Shin [a], Jaehan Im [a], Ji-Woong Choi [a], Hyun Sik Kim [b], Jung Inn Sohn [c],

*Seung Nam Cha [c], and Jae Eun Jang [a,]**

[a]*Department of Information and Communication Engineering, Daegu Gyeongbuk Institute of Science and Technology (DGIST), Daegu, 711-873, Korea,*

[b]*Department of Applied Physics and Material Science, California Institute of Technology, Pasadena, CA 91125, U.S.A,*

[c]*Department of Electrical Engineering Science, University of Oxford, Park Road, Oxford, OX1 3PJ, U. K,*

*Corresponding authors. Tel: +82 53 785-6312. E-mail: jang1@dgist.ac.kr

KEYWORDS MIM diode, MIC diode, tunneling effect, field enhancement factor, carbon nanotube

ABSTRACT Ultra-fast diode structures based on non-semiconductive materials employing tunneling mechanism have been investigated. Applying the structurally asymmetric effect of multi-wall carbon nanotube (MWCNT) to a vertical metal-insulator-MWCNT (MIC) tunneling diode structure, the 'on-off' ratio (~10^4) and the current density (38.2MA/cm^2) are drastically enhanced compared to those of conventional metal-insulator-metal (MIM) tunneling diodes. The electrical characteristics are stable up to 423K. Experimentally, rectifying performance of the MIC diode is good up to 10MHz and the cut-off frequency of the MIC diode is estimated to be 6.47THz. The growth process of MWCNT is more controllable for the number and the position than that of SWCNT. Therefore, it has a high probability of realization. The vertically aligned single MWCNT design can guarantee an ultra-high integration density, as well. Therefore, the MIC diode can be applied to various high frequency applications, such as communication devices, high speed electrical switches, and high performance control process units (CPUs), or other new concept devices.

1. Introduction

Recently, ever-increasing demand for faster electronic devices in various fields has drastically improved their driving speed. Typically, the driving frequency of electronic communication devices has gradually increased from kilohertz (KHz) to gigahertz (GHz) level over the past decade. However, with the advent of smartphones a much higher driving frequency is required to store more information into electro-magnetic waves; it will approach terahertz (THz) level, as soon. High speed electrical switch working at THz frequency should be developed as well for a high performance control process unit (CPU), for which a Si based field-effect transistor (FET) is commonly used, since the current maximum driving speed is

around 1~2GHz [1]. Many new electrical device concepts utilizing optical approaches, among which is a rectenna, have been suggested for an even higher driving frequency. When the rectenna, an antenna-coupled rectifier, is applied as one of new solar cell concept, the solar cell is expected to have a much higher efficiency than a conventional one with estimated driving frequency of tens to hundreds THz [2]. For these high-speed electrical devices to perform at their best, an ultra-fast driving diode is required as their basic electrical unit. A *p-n* junction diode structure has been widely used, which is also a core component in a Si based transistor. However, its working mechanism is not suitable for high-speed driving since its speed is limited by mobility of holes and electrons in a semiconductor [3]. A Schottky diode has a much faster rectifying speed than that of the *p-n* junction diode due to one side depletion formed by movement of holes or electrons alone [4, 5]. Nonetheless, its maximum driving frequency is estimated to be less than one or two THz. Furthermore, flows of electrons through the Schottky barrier via thermionic injection lead to a poor power efficiency, which is regarded as important in mobile devices [6]. Although a tunneling diode using metal-metal or semiconductor-semiconductor junction can be chosen to avoid thermionic emission, low conversion efficiency and driving speed retardation due to its high reverse current level are inevitable [7-23]. Here we report a tunneling diode structure using metallic multi-wall carbon nanotube (MWCNT) as one of the electrodes in the structure with high contrast between a reverse current and forward current. The structural asymmetric effect from nano-sized MWCNT makes a large difference in the tunneling probability, the barrier height, and the width for the forward bias and reverse bias [9, 24, 25].

2. Experimental part

2.1 Fabrication of simple metal-insulator-metal (MIM) diode

The simple MIM diode was fabricated on Si/SiO_2 (1000 Å) to prevent the devices from unexpected leakage current that leads to low performance. All patterns were formed by photolithography and lift-off. Al (4N of purity), Ni (4N5 of purity), and Pt (4N of purity) were deposited by sputtering system. We employ native oxide to form insulator layer. Aluminum and nickel are to easily get thin native oxide, as thin as 56Åm measured in Hitachi HF-3300 TEM, as shown in Fig. S1.

2.2 Fabrication of lateral metal-insulator-metal (MIM) diode

The Si/SiO_2 (1000 Å) is used as a base substrate to block unexpected current from other path ways, same as simple MIM diode. The fabrication is composed of photolithography and electron beam lithography (EBL) for pad and sharp tip shape, respectively. It commonly employs PMMA (polymethyl methacrylate) that is very sensitive to high energy electrons for direct write EBL. JEOL JBX-9300FS E-beam lithography was used for a sharp tip. Nb and Pt were used for flat and sharp tip electrode and deposited by sputtering system. SiO_2 layer is also defined by photolithography and sputtering system. More details about fabrication of lateral MIM diode is descripted in Fig. S2.

2.3 Fabrication of metal-insulator-carbon nanotube (MIC) diode

The same substrate is used for MIC diode as simple and lateral MIM diode. AZ GXR 601 was coated as 1um thickness and was exposed with $60mJ/cm^2$ dose. Sputtering system was used to deposit Nb of 150nm thickness and then lift-off process was carried out with acetone. A cycle

of this fabrication based on photolithography and lift-off was repeated to form oxide layer with opening bottom electrode. For the MWCNT grown by dc-PECVD, the density can be controlled by the size of catalyst. Through our previous result, we can grow a single carbon nanotube using dot-type catalyst of which diameter is several hundred nanometer [26]. A single MWCNT can be grown from bellow 400nm diameter. However, for high yield of single MWCNT, the diameter is appropriate below 200nm. In here, the diameter was chosen as 100nm~120nm. To make Ni catalyst with the diameter, E-beam lithography was carried out using JEOL JBX-9300FS with 400 uC/cm^2 dose after PMMA A3 950K, E-beam resist, was coated to make 90nm thickness. Ni deposition (20nm thickness) and lift-off process were performed by thermal evaporator system with deposition ratio of 0.5Å/sec and with acetone, respectively. For growth of a vertical multi-wall carbon nanotube (MWCNT), plasma enhanced chemical vapor deposition by AIXTRON's Black Magic 2 inch system was used with an optimized condition. After pump-out up to 6mbar, the graphite substrate was heated up from room-temperature to 555°C with 50°C/min ramp-up speed. After 55sccm of C_2H_2 was injected into the chamber, it was heated up again from 555°C to 565°C with 200°C/min. After keeping the state for 60 seconds, plasma of 600V was induced for 5minutes. SU-8 was coated as thick as 1.5um to sustain the top electrode at the top of a vertical MWCNT. Photolithography was performed with 70mJ/cm^2 dose and O_2 plasma then was carried out with 100W power and 100 sccm of O_2 for 30 sec to open the top of carbon nanotube. After removing SU-8 at the top of MWCNT, the top electrode was fabricated. Photolithography was performed with the same condition to form the bottom electrode. Al (approximately 300nm) was deposited and lift-off process was carried out with acetone. More details about fabrication of MIC diode is descripted in Fig. S3 and the details of growth process can be found elsewhere [26-28].

3. Results and discussion

3.1 Electrical characteristics

A metal-insulator-metal (MIM) tunnel diode, where a quantum mechanical effect takes place, is capable of high-speed rectification. Two different metals, which have different work functions, can have asymmetric current-voltage (I-V) characteristics [29-31]. To investigate the effect of work function difference, simple MIM diodes were fabricated using Al-AlO_x-Al, Ni-NiO_x-Ni, and Al-AlO_x-Pt layers. Fig. 1a shows schematic illustrations of the simple MIM diodes.

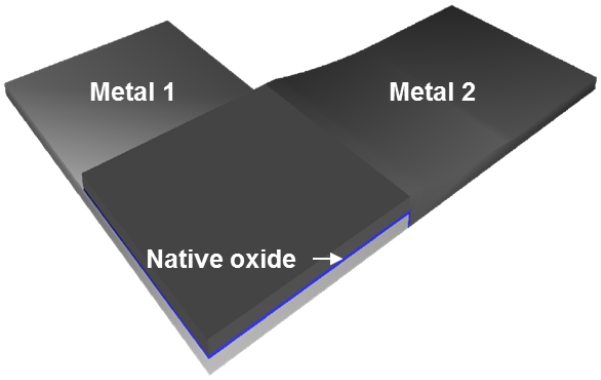

(a)

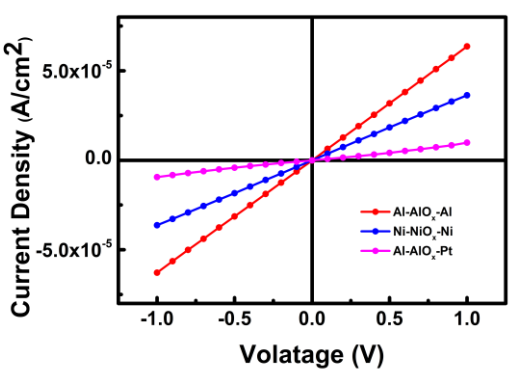

(b)

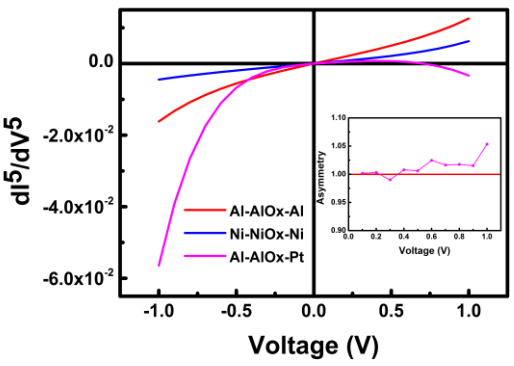

(c)

Fig. 1. Schematic diagram of the simple MIM diode and its electrical characteristics. (a) Diagram of the simple MIM diode. (b) Current density-Voltage plot with voltage range from -1 to 1V and (c) Fifth-order differentiation and inset: Asymmetry of simple MIM diode ($I_+/|I_-|$) of Al-AlO_x-Pt.

The band diagram presents a work function difference between two metals, Al-AlO_x-Al, Ni-NiO_x-Ni, and Al-AlO_x-Pt in Fig. S4. Symmetric work function was built in Al-AlO_x-Al and Ni-NiO_x-Ni. In contrast, Al-AlO_x-Pt structure has different barrier formations compared to the oxide-metal interface by 1.37eV. Al-AlO_x-Al and Ni-NiO_x-Ni have symmetric I-V characteristics at negative to positive bias sweep in Fig. 1b. Al-AlO_x-Pt structure has more asymmetric characteristics than these symmetric structures. Fig. 1c shows fifth-order differentiation to amplify difference between negative and positive bias. Even though the 1.37eV could build asymmetry in Fig. 1c, the order of asymmetry between the negative bias and positive bias of the MIM diode is 1.05 (Fig. 1c inset). Although the structure may drive at THz region due to tunneling driving mechanism, the work function difference between the metals cannot produce a high asymmetry in an I-V plot; this can lead to an inefficient performance for rectifying or electrical switching. To enhance the asymmetric behavior in the I-V curve, a structural effect is considered. For a flat metal and an insulator (or vacuum) under electrical field, the potential energy (PE) can be written as [4]

$$PE_{M\to O}(x) = (E_F + \phi) - \frac{e^2}{16\pi\varepsilon_0 x} - exE \tag{1}$$

where E_F, ϕ, ε_0, x and E are the Fermi level, work function, absolute permittivity, distance from surface, and the electrical field. However, if a sharp or high aspect ratio metal structure is utilized as one of electrodes instead of the flat metal, the PE equation is also changed to include β, the field enhancement factor (2).

$$PE_{M\to O}(x) = (E_F + \phi) - \frac{e^2}{16\pi\varepsilon_0 x} - \beta exE \tag{2}$$

The PE bends steeply to give rise to a narrow PE barrier. The corresponding tunneling probability is derived as

$$T = T_o exp\left(-\alpha \frac{E_F + \phi + \sqrt{(E_F + \phi)^2 - \beta E \frac{e^3}{\pi \varepsilon_0}}}{\beta e E}\right) \quad (3)$$

where T_o is the pre-exponential constant and $\alpha^2 = 2m(V_O - E)/\hbar^2$. The sharp metal structure induces a low tunneling-voltage with higher tunneling current. Therefore a much more asymmetric I-V curve can be obtained by changing shape of the metal, which, in turn, alters the β value; a sharp or high aspect ratio structure gives a higher β. It can be increased to 20000 for nanowires or nanotube structures [4].

The lateral asymmetric structure is designed to apply the idea to the diodes structure. Fig. 2a shows the schematic illustration of the lateral MIM diode structure.

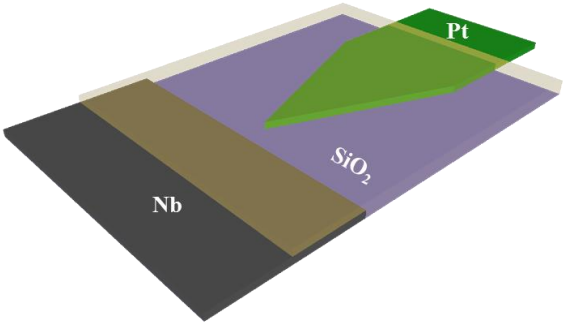

(a)

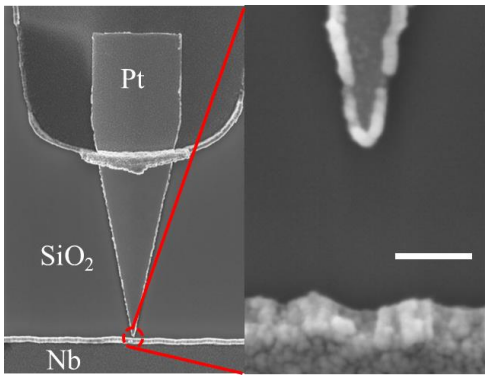

(b)

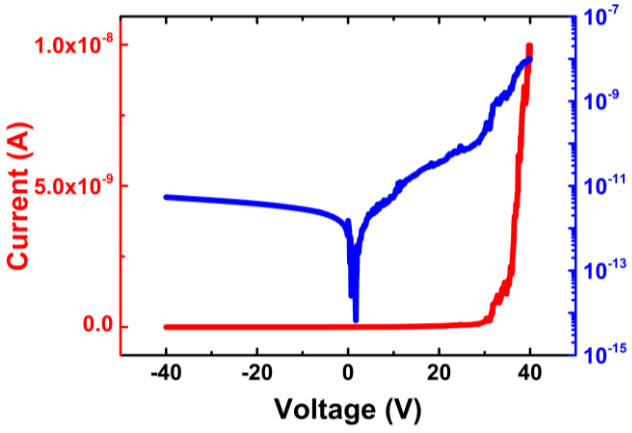

(c)

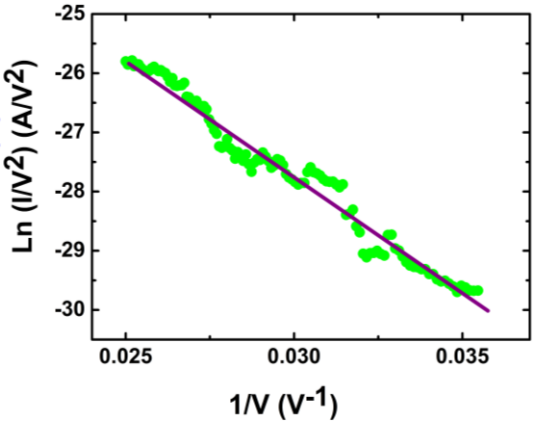

(d)

Fig. 2. The lateral MIM diode structure and the electrical characteristics. (a) Schematic diagram of the lateral MIM diode composed of Nb-SiO_2-Pt on the SiO_2/Si substrate. (b) SEM images; top view of whole device (left-image) with bonding pad and magnified view (right-image). The scale bar is 20nm. (c) Left axis: current-voltage plot from -40 to 40V. Right axis: log scale plot of current-voltage measurement. (d) The plot based on Fowler-Nordheim tunneling model.

The process details describe in the experimental part and supporting information. The structure consists of a flat metal and a sharp tip-like structure for the structural asymmetry effect. To give more asymmetry effect from the work function difference of materials, Nb and Pt were used for the flat and the sharp metal, respectively. SiO_2 layer deposited between Nb and Pt is the main pathway of electron and the tunnel junction. The electron can be easily moved between the sharp metal and the flat metal by the field-effect tunneling. The tunneling probability can be controlled by the electrode structure. The important merit of the device is the simple design and the easy fabrication process. The SEM images show whole Nb-SiO_2-Pt lateral MIM diode including bonding pad in Fig. 2b. The gap between the flat metal and the sharp tip is approximately 40nm. The electrical characteristics of the lateral MIM diode are shown in Fig. 2c. This graph shows much more asymmetric I-V curve than that of the simple MIM diode. Applying negative bias to the lateral MIM diode, the current flow is blocked by the low tunneling probability. At positive bias, the current flow is occurred by field-effect tunneling, proved by straight line in Fowler-Nordhiem tunneling plot (Fig. 2d). Although it has a good rectifying characteristics and tunneling effect, the threshold voltage is as high as 30V and the current is small due to high resistance from the wide gap size. Since the process needs two more steps for the fabrication of device using two type metals, the gap between electrodes decided by the align accuracy of e-beam lithography system and the lithography conditions is not narrow. Even though the tip structure has a good sharpness (r: ~5nm), the electrical characteristics is so poor. The tunneling SiO_2 layer can be other reason for the problem. The

SiO_2 layer formed by sputtering method can make the poor surface interface or the void between the tip and SiO_2 film. If we can make much smaller gap between electrodes with a high quality oxide layer, the lateral MIM structure will have more enhancement for the rectifying effect.

Therefore, a carbon nanotube (CNT), especially vertically aligned MWCNT is an ideal candidate for an electrode since it has a high aspect ratio from its own structure, good electrical conductivity for high frequency alternating current (AC) signal, small capacitance from a small junction area, and an easy fabrication process for structures in nanoscale. Until now, most of researches employing CNT for diode or triode structure have used semi-conductive single wall CNT (SWCNT) to make use of *p*-*n* junction or Schottky barrier as a main working principle. As mentioned above, the *p*-*n* junction and the Schottky barrier are not suitable for ultra-high speed driving, and moreover, number of CNTs and their spatial points cannot be controlled precisely by any currently available growth technology. However, a vertically aligned single MWCNT grown by plasma enhanced chemical vapor deposition (PECVD) with nano-sized catalyst pattern is one of a few controllable bottom-up growth structures for nano-devices. Moreover, although the MWCNT has been considered hard to be applied to electrical switches due to metal-like electrical property, it can be a good merit of MWCNT applied to MIM tunneling effect.

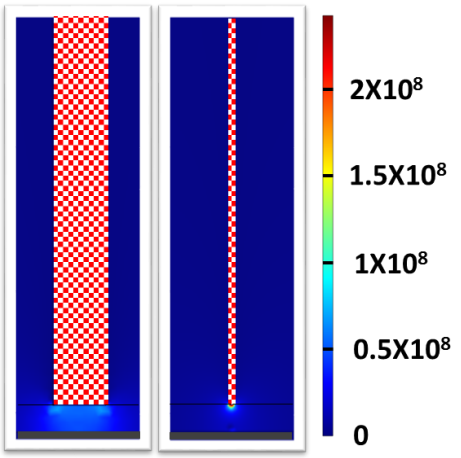
2X10^8
1.5X10^8
1X10^8
0.5X10^8
0

(a)

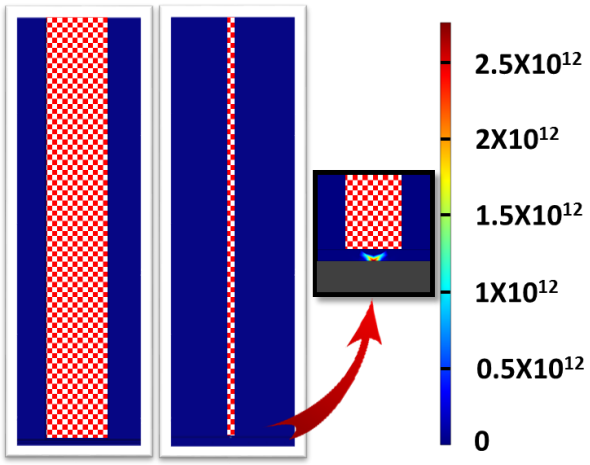
2.5X10^12
2X10^12
1.5X10^12
1X10^12
0.5X10^12
0

(b)

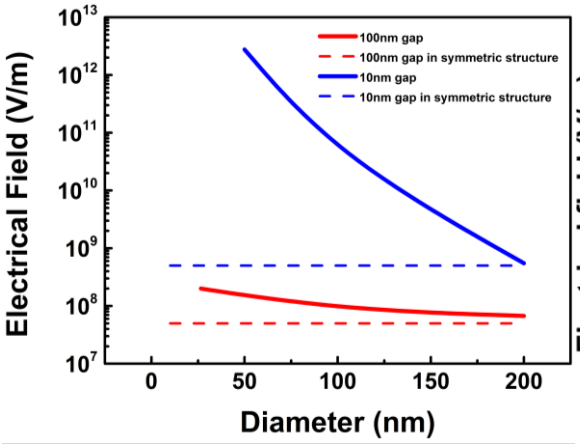
Electrical Field (V/m)
Diameter (nm)
100nm gap
100nm gap in symmetric structure
10nm gap
10nm gap in symmetric structure

(c)

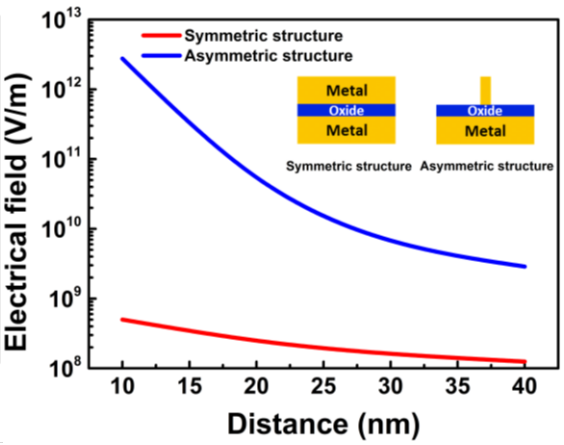
Electrical field (V/m)
Distance (nm)
Symmetric structure
Asymmetric structure
Metal
Oxide
Metal
Oxide
Metal
Symmetric structure
Asymmetric structure

(d)

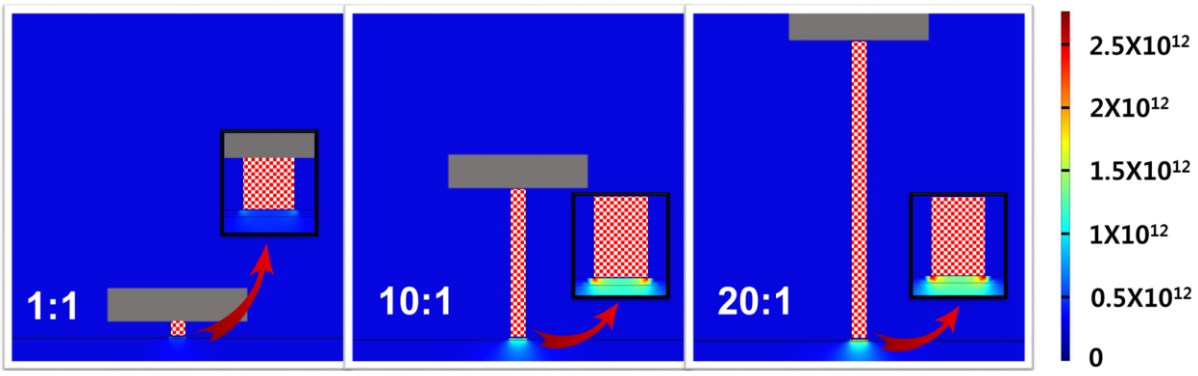
1:1
10:1
20:1
2.5X10^12
2X10^12
1.5X10^12
1X10^12
0.5X10^12
0

(e)

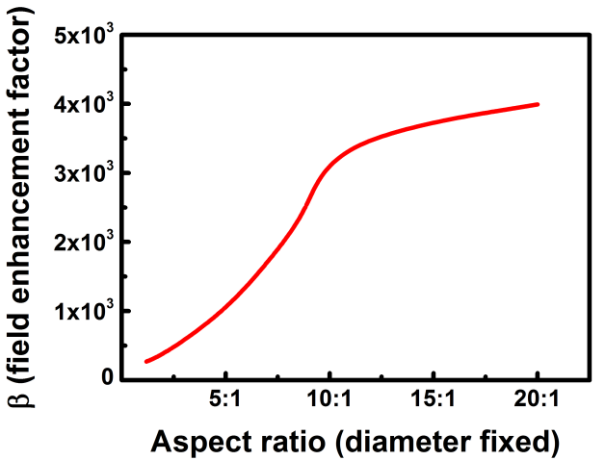

(f)

Fig. 3. Vertical MIC diode structure, the simulation results of electrical field using COMSOL (a) The simulation of electrical field in asymmetric structure, metal (bottom electrode – flat) – insulator (SiO_2-100nm) – metal (Nanowire type-high aspect ratio electrode): 200nm and 50nm (b) with insulator (SiO_2-10nm) and 200nm and 50nm of diameter (c) The graph of electrical field (maximum electrical field) relying on diameter of top electrodes in 100nm and 10nm gap. The dash line shows that of symmetric electrodes. (d) The comparison of dependence of electrical field on distance between bottom and top electrode in symmetric and asymmetric structure. (e) The simulation of electrical field with various diameter fixed aspect ratio (1:1 & 10:1 & 20:1) depending on length (diameter: 75nm fixed) (f) The graph of β (field enhancement factor) relying on aspect ratio (diameter fixed)

Fig. 3a shows electrical field simulation of the MIC structure. Strong localized electrical field distribution in insulator layer between carbon nanotube and metal is induced by the high aspect ratio structure (relying on diameter) of the CNT (Fig. 3 a, b). The length of nanowire type-high aspect ratio electrode is fixed to 1.5um. The diameter of MWCNT can be controlled by the size of catalyst and growth conditions. Considering the largest catalyst size to get single MWCNT on selected position, 200nm diameter is maximum. As decreasing the diameter of MWCNT, induced electrical field is increased due to the higher aspect ratio of CNT. The order of electrical enhancement depends on the gap, as well. In case of symmetric structure, the electrical field simply inversely proportional to the thickness of oxide. For example, applying 5V to an electrode, the symmetric structure with 10nm and 40nm of oxide thickness can have 5×10^8 and 1.25×10^8 V/m of electrical field, respectively, according to E (electrical field) $\propto 1/d$ $(distance)$ relationship. However, in case of asymmetric structure, the reduction of oxide thickness induces quite higher electrical field. The electrical field in asymmetric structure with

10nm oxide thickness is about 2.8 × 10^{12} V/m as shown in Fig. 3c and 3d. Much stronger electrical field can be enhanced by smaller diameter of MWCNT and thinner oxide layer. The calculated β field enhancement factor from simulation results is about 5519. The increase of tunneling probability from the high β value can make higher current flow for the positive bias states.

To find appropriate length of MWCNT, the electrical field with various aspect ratio of CNT were calculated by simulation program (COMSOL), as shown in Fig. 3e. The diameter of CNT in simulation was fixed to 75nm due to the real diameter of multi-wall carbon nanotube in MIC structure and oxide thickness between two metals is 10nm. With the change of aspect ratio from 1:1 to 20:1, the tendency of electrical field and β value were investigated. In case of 1:1 aspect ratio, electric field between two metals (in insulator layer) is quite low; however, that of 10:1 and 20:1 aspect ratio structure is stronger than 1:1 aspect ratio structure. The plot of β value depending on aspect ratio (diameter fixed) is shown in Fig. 3f. Even though the slope of 1:1 to 10:1 aspect ratio structure drastically increase, over 10:1 aspect ratio, it shows a gentle slope and it is almost saturated from 20:1. It indicate that high electrical field enhancement can be achieved at least 10:1 aspect ratio structure. High aspect ratio structure over 10:1 is not achieved easily in nanometer scale. For 'top-down' approach which is formation of metal cylinder structure using lithography and etching process, considering length, the structure of 10:1 (750nm length and 75nm diameter) aspect ratio is not easy to be obtained even using e-beam lithography. However, if we choose 'bottom-up' process, the growth of carbon nanotube, it can be easily achieved the aspect ratio as high as over 10:1. The aspect ratio of 20:1 (diameter: 75nm and length: 1.5um) can be successfully acquired in MIC diode and calculated β value is 3993.

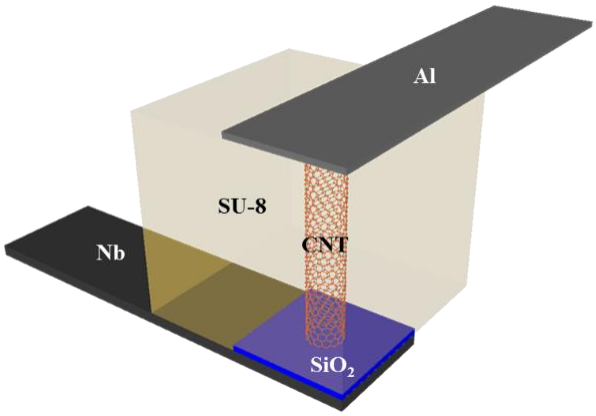
Al
SU-8
CNT
Nb
SiO2

(a)

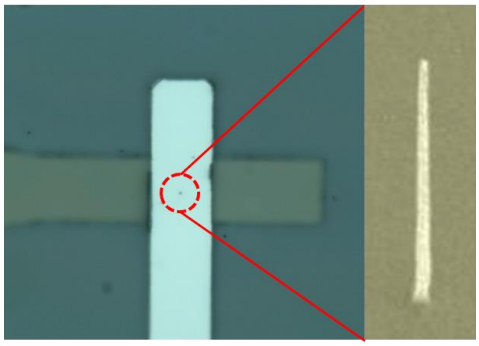

(b)

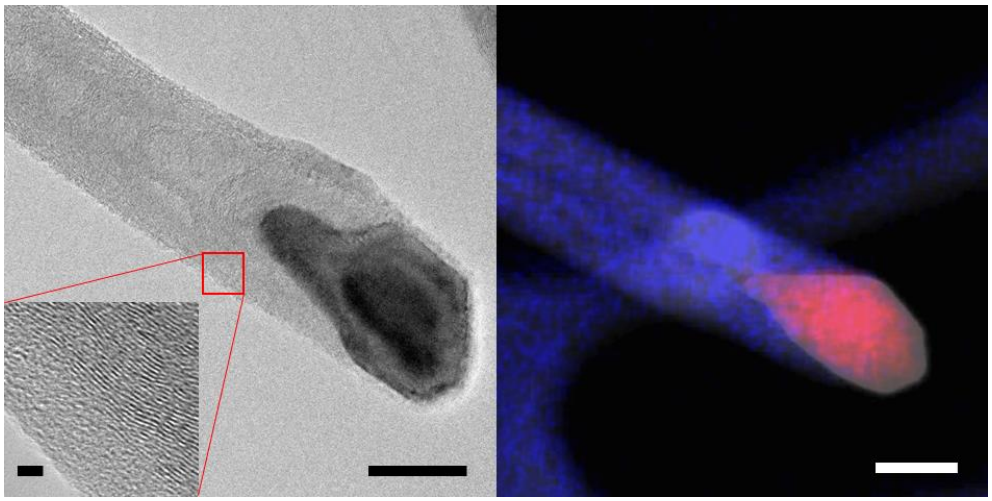

(c)

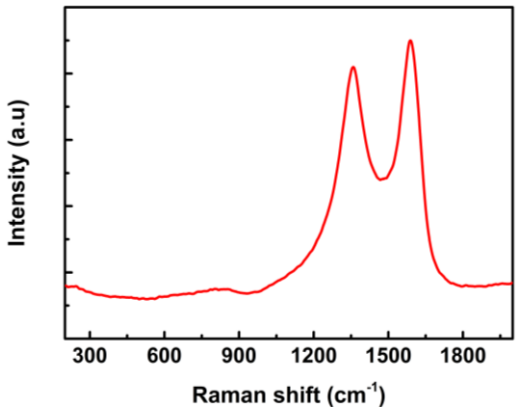
Intensity (a.u)
300
600
900
1200
1500
1800
Raman shift (cm-1)

(d)

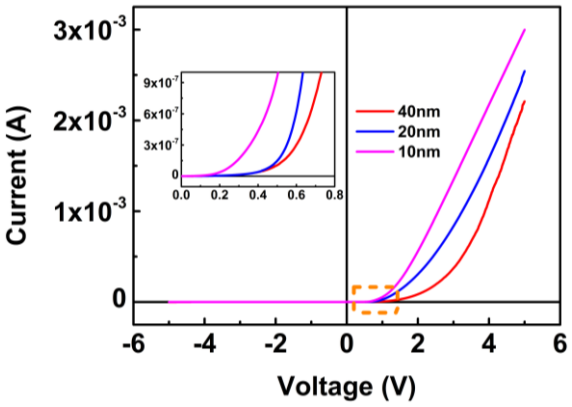
3x10-3
2x10-3
1x10-3
0
Current (A)
-6
-4
-2
0
2
4
6
Voltage (V)
40nm
20nm
10nm

(e)

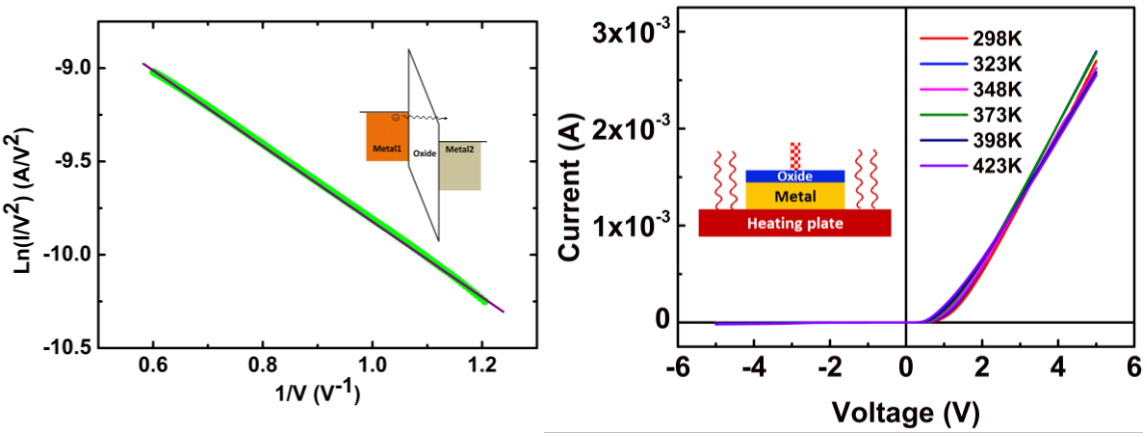

(f) (g)

Fig. 4. Vertical MIC diode structure and electrical characteristics. (a) Schematic diagram of the MIC diode composed of Nb-SiO_2 Carbon nanotube on the SiO_2 substrate. (b) The optical photo image of MIC structure. The point inside the red circle is the vertical MWCNT. The inset: 45° tilted view of SEM image for a multi-wall carbon nanotube grown on SiO_2/Nb layers. (c) The TEM (Hitachi HF-3300 TEM) image of MWCNT (left) and EDS mapping (right) of carbon and nickel; blue: carbon and red: nickel. The scale bar is 50nm (left and right images). The inset (left): a magnified image of wall of MWCNT. The scale bar is 2nm. (d) The Raman spectrum of MWCNT grown by dc-PECVD with Ni catalyst. (e) Current-Voltage plots of MIC diodes. The inset of the plots: threshold plots with 10, 20, 40nm (thickness of SiO_2) MIC diodes with magnified voltage-axis from 0 to 0.8V. (f) The plot based on Fowler-Nordheim tunneling model in the sample with 10nm SiO_2. (g) The I-V plot of temperature-dependence of MIC diode from 298K to 423K.

Fig. 4a shows a schematic image of suggested device design. After formation of Nb flat bottom electrode, thin SiO_2 layer was deposited. A SiO_2 layer between the flat metal and the MWCNT acts as a tunneling medium. The film thickness of the SiO_2 layer corresponds to the tunneling gap of the device due to its vertical design concept. The film thickness is easily controlled by a deposition system with 1nm resolution. This is one of important merits for the vertical design compared to the lateral MIM structure. A single MWCNT was grown by catalyst assisted PECVD process. To make the top contact electrode, a planarization layer was formed by SU-8.

Fig. 4b shows the optical microscope image of MIC diode and SEM image of a CNT at center of overlapped junction. To apply CNT to real device formation, the population control and the selective growth are essential requirements. A single vertical MWCNT is grown on selected point with the precise control of catalyst size and plasma enhanced chemical vapor deposition system (PECVD). More details about fabrication of MIC diode is descripted in Fig. S3 and the details of growth process can be found elsewhere [26-28].

The characterization of MWCNT grown by using dc-PECVD are shown in Fig. 4c and d. Fig. 4c shows TEM analysis of the MWCNT with EDS mapping. According to the TEM image, it is one of general growth structure using dc-PECVD [32]. The electrical conductivity of the MWCNT is quite good; thus, the MWCNT is promising as one of materials for high speed devices [33]. The aspect ratio and conductivity of CNT are main important factors for the MIC diode application. A single MWCNT grown by dc-PECVD with catalyst size control skill is one of the best candidate in these points. Through TEM analysis with EDS mapping of nickel and carbon, the Ni catalyst positioned at the top of MWCNT. Therefore, the properties of Ni such as the work function level do not affect significantly to the electrical characteristic of MIC structure [26]. CNT has D band and G band in Raman spectrum at ~1340 cm^{-1} and ~1600 cm^{-1}, respectively. Fig. 4d corresponds well to that of general MWCNT.

Fig. 4e shows I-V characteristics of the MIC structures with different oxide thicknesses. The threshold voltage and current level are drastically improved. The threshold voltage drops below 0.5V for all oxide cases. For 10nm SiO_2 case, the threshold voltage is lower than 0.2V. The current flow is also increased to ~3mA at 5V. The strongly enhanced electrical field, which is induced by a high aspect ratio of CNT, thin oxide thickness and good surface interface between CNT and SiO_2 are the reasons for the improvement. From the junction dimension decided by the radius of CNT, the current density is 38.2MA/cm^2, which is considerably higher than that of a conventional MIM diode structure. The leakage current level is slowly increased from 10^{-}

^{10}A to 10^{-7}A when up to -5V bias is applied; similar behavior can be observed in most oxide structures. The 'on-off' ratio between the forward current and the reverse current level is ~10^4. For other tunneling diodes, for example, 'on-off' ratio of MIM or highly doped *p-n* tunneling diode is smaller than 10^2 [10-12, 21]. Therefore, the newly suggested MIC diode structure has good rectifying efficiency with high current level. The straight line in the plot based on Fowler-Nordhiem tunneling model (Fig. 4f) indicates that the current flow is mainly induced by the tunneling effect. To make sure the current path in MIC diode, MIC diode without CNT was fabricated and measured electrical characteristics, as shown in Fig. S6. The current level is about 10^{-13}A. Thus, we make sure the main electron path is CNT. Fig. 4g shows the thermal stability of the MIC diode. From room temperature to 423K, the I-V characteristics follow a similar trend. Although the thermal effect of the tunneling diode is smaller than *p-n* junction diode, general tunneling diode has poor conversion efficiency at high temperature due to its originally low 'on-off' ratio. For MIC structure, structurally asymmetric effect is not theoretically affected from the thermal effect. Therefore, the structure maintains the asymmetric I-V characteristics and the high conversion efficiency at even high temperature. The thermal stability of MIC structure extends its applications to IR/THz detector or the electrical switch for automobile, where the structure is required to be reliable at high temperature. We also experimentally calculated β value in MIC diode. The value of 10nm SiO_2 case is as high as about 17000, which is much higher than the simulation result (Fig. 3f). In the simulation, simplified cylindrical model was chosen for CNT structure. However, real CNT structure is close to a tube type structure rather than a cylinder type filled. Therefore, it is assumed that the tube like structure of CNT induces much higher value than simulated results. The β value is an important factor to induce high 'on-off' ratio, current density, and cut-off frequency. The structure of MIC diode can be available to drive high frequency.

3.2 Rectifying performance

We investigated the rectifying behavior and the cut-off frequency under AC bias state for various diodes. Those factors were measured by two channel oscilloscope and a wave form generator. Even though these are important factors to estimate performance of diode characteristics, most results with high frequency diode mainly consider low resistance and capacitance for cut-off frequency. Fig. 5 shows the rectifying performance of the various diodes in a frequency range from 60Hz to 10MHz for simple MIM, lateral MIM, and MIC diodes in comparison to a commercial Schottky diode (1N5817).

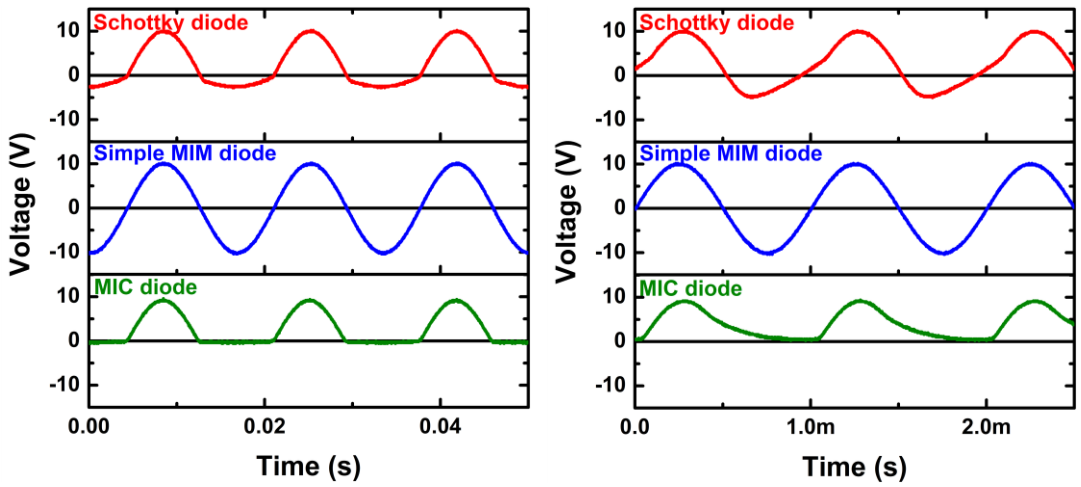

(a) (b)

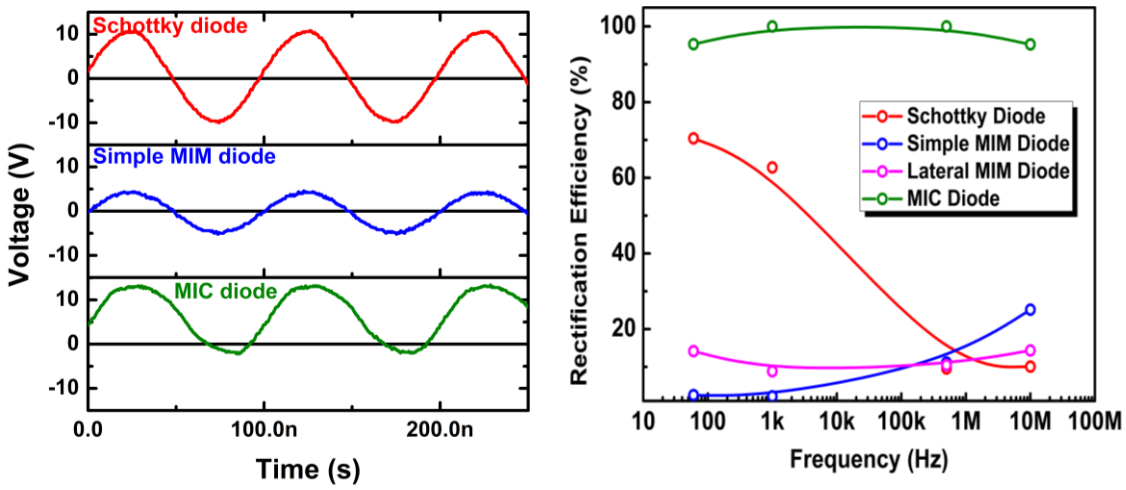

(c) (d)

Fig. 5. Rectifying performance of the commercial Schottky diode (red-line), simple MIM diode (blue-line), and the MIC diode (green-line) (a) The rectifying performance at 60Hz, (b) 1kHz, and (c) 10MHz. The voltage signal on pink color region corresponds to the reverse current flow at the negative bias signal. (d) The graph of rectification efficiency from 60 Hz to 10MHz.

As inferred from I-V characteristics of those structures, the simple MIM diode does not show a rectifying performance for AC sinusoidal wave, even at 60Hz (Fig. 5a). The output signal is almost the same as the input signal. Commercial Schottky diode shows a rectification performance at low frequency driving. However, -2.5V output bias is detected for -10V input signal, mainly due to its original reverse current and the conductance mechanism. The MIC structure makes an ideal 'off' state for negative input region. The output signal is identical to the positive input signal. In case of Schottky diode, as increasing frequency, much bigger negative region can be shown in Fig. 5b and c. Fig. 5d shows rectification efficiency, which indicate that how much it can convert AC signal to DC signal. The rectification efficiencies of simple MIM diode and lateral MIM diode are below 30% from 60Hz to 10MHz due to symmetric I-V characteristics and threshold voltage as high as 30V, respectively. Although Schottky diode has high rectification efficiency over 70% at low frequency range, as increasing

frequency this factor dramatically decrease down to 10%. In the other words, Schottky diode cannot block negative current at high frequency range. MIC diode can keep high rectification efficiency over 90% up to 10MHz. It is expected to have higher potential to drive efficiently for ultra- high frequency AC signal. Considering electrical property of CNT, it is one of the suitable materials to drive high frequency signal [34]. Thus, the MIC structure can be a good candidate for a rectifying component to ultra-high frequency with small threshold voltage. The ideal driving frequency limit is estimated to be $1/2\pi RC$, where R and C are the resistance of junction layer and the capacitance between Nb and MWCNT, respectively. These parameters, R and C, were obtained from I-V curve and COMSOL simulation in Fig. S8, respectively. To secure more appropriate capacitance, the simulation from 3D model was performed and the value is 1.4725×10^{-17}F. By using values of R = 1.67kΩ and C = 1.4725×10^{-17}F, the estimated frequency limit is as high as 6.47THz.

4. Conclusions

Ultra-fast diodes based on all metallic structures employing tunneling mechanism have been investigated. Applying the asymmetric structure effect to MIM diodes, a better electrical asymmetric characteristic was achieved in the MIC structure. High contrast ratio between on- and off-current is as high as about forth-order at room temperature. Its temperature dependence is stable up to 423K, compared to the other results. In addition, rectifying performance of the MIC diode through AC signal is good up to 10MHz with few negative current. The estimated cut-off frequency of the MIC diode is 6.47THz. Ultra-fast structural asymmetric diode using all metallic materials can be applied to various high frequency applications, such as communication devices, high speed electrical switches, energy harvesting structures, and so forth as high performance tunnel diodes.

Acknowledgments

This research was supported by the National Research Foundation of Korea (NRF) grant funded by the Korea government (MSIP) (2015R1A2A2A01005043) and DGIST R&D Program of MSIP (16-BD-0404)

Appendix A. Supplementary data

Supplementary data associated with this article can be found, in the online version, at http://

REFERENCES

[1] Dragoman D, Dragoman M. Terahertz fields and applications. Prog Quantum Electron. 2004;28(1):1-66.
[2] Berland B. Photovoltaic technologies beyond the horizon: optical rectenna solar cell. National Renewable Energy Laboratory Final Report 2003 [cited 2003 Feb]; Available from: http://www.nrel.gov/docs/fy03osti/33263.pdf.
[3] Sedra AS, Smith KC. Microelectronic circuits. 6th ed. New York: Oxford University Press; 2010.
[4] Kasap SO. Principles of electronic materials and devices. 3rd ed. New York: McGraw-Hill 2006.
[5] Sze SM, Ng KK. Physics of semiconductor devices. 3rd ed. New York: Wiley-interscience; 2006.
[6] Ionescu AM, Riel H. Tunnel field-effect transistors as energy-efficient electronic switches. Nature. 2011;479(7373):329-37.
[7] Reddick WM, Amaratunga GA. Silicon surface tunnel transistor. Appl Phys Lett. 1995;67(4):494-6.
[8] Appenzeller J, Lin Y-M, Knoch J, Avouris P. Band-to-band tunneling in carbon nanotube field-effect transistors. Phys Rev Lett. 2004;93(19):196805.
[9] Bjork M, Schmid H, Bessire C, Moselund K, Ghoneim H, Karg S, et al. Si–InAs heterojunction Esaki tunnel diodes with high current densities. Appl Phys Lett. 2010;97(16):163501--3.
[10] Bessire CD, Björk MT, Schmid H, Schenk A, Reuter KB, Riel H. Trap-Assisted Tunneling in Si-InAs Nanowire Heterojunction Tunnel Diodes. Nano Lett. 2011;11(10):4195-9.
[11] Ganjipour B, Dey AW, Borg BM, Ek M, Pistol M-E, Dick KA, et al. High current density Esaki tunnel diodes based on GaSb-InAsSb heterostructure nanowires. Nano Lett. 2011;11(10):4222-6.
[12] Georgiou T, Jalil R, Belle BD, Britnell L, Gorbachev RV, Morozov SV, et al. Vertical field-effect transistor based on graphene-WS2 heterostructures for flexible and transparent electronics. Nat Nanotechnol. 2012;8(2):100-3.
[13] Li J, Zhang Q, Chan-Park MB. Simulation of carbon nanotube based p–n junction diodes. Carbon. 2006;44(14):3087-90.
[14] Mookerjea S, Mohata D, Krishnan R, Singh J, Vallett A, Ali A, et al. Experimental demonstration of 100nm channel length $In_{0.53}Ga_{0.47}As$-based vertical inter-band tunnel field effect transistors (TFETs) for ultra low-power logic and SRAM applications. Electron Devices Meeting (IEDM): IEEE; p. 1-3.
[15] Britnell L, Gorbachev R, Jalil R, Belle B, Schedin F, Mishchenko A, et al. Field-effect tunneling transistor based on vertical graphene heterostructures. Science. 2012;335(6071):947-50.
[16] Kim S, Shin DH, Kim CO, Kang SS, Kim JM, Jang CW, et al. Graphene pn Vertical Tunneling Dodes. ACS nano. 2013;7:5168-74.
[17] Krishnamoorthy S, Kent TF, Yang J, Park PS, Myers RC, Rajan S. GdN Nanoisland-Based GaN Tunnel Junctions. Nano letters. 2012;13:2570-5.
[18] Li J, Zhang Z, Kwong G, Tian W, Fan Z, Deng X. A new exploration on the substantial improvement of rectifying behaviors for a donor–acceptor molecular diode by graphene electrodes. Carbon. 2013;61:284-93.
[19] Tongay S, Schumann T, Miao X, Appleton B, Hebard A. Tuning Schottky diodes at the many-layer-graphene/semiconductor interface by doping. Carbon. 2011;49(6):2033-8.

[20] Zhao H, Chen Y, Wang Y, Zhou F, Xue F, Lee J. InGaAs tunneling field-effect-transistors with atomic-layer-deposited gate oxides. IEEE Trans Electron Devices. 2011;58(9):2990-5.
[21] Yu WJ, Li Z, Zhou H, Chen Y, Wang Y, Huang Y, et al. Vertically stacked multi-heterostructures of layered materials for logic transistors and complementary inverters. Nat Mater. 2012;12(3):246-52.
[22] Salomon A, Boecking T, Seitz O, Markus T, Amy F, Chan C, et al. What is the Barrier for Tunneling Through Alkyl Monolayers? Results from n-and p-Si‐Alkyl/Hg Junctions. Adv Mater. 2007;19(3):445-50.
[23] Li J, Zhang Z, Qiu M, Yuan C, Deng X, Fan Z, et al. High-performance current rectification in a molecular device with doped graphene electrodes. Carbon. 2014;80:575-82.
[24] Deb P, Kim H, Qin Y, Lahiji R, Oliver M, Reifenberger R, et al. GaN nanorod Schottky and pn junction diodes. Nano letters. 2006;6(12):2893-8.
[25] Sun X. Designing efficient field emission into ZnO. SPIE Newsroom, The International Society for Optical Engineering, s 1C4. 2006.
[26] Im J, Kim S, Shin JH, Choi Y, Cha SN, Jang JE. High Growth Yield of Single Multiwall Carbon Nanotube With Different Length Effect. IEEE Trans Nanotech. 2014;13(2):316-21.
[27] Jang JE, Cha SN, Choi Y, Kang DJ, Hasko DG, Jung JE, et al. A nanogripper employing aligned multiwall carbon nanotubes. Nanotechnology, IEEE Transactions on. 2008;7(4):389-93.
[28] Jang JE, Cha SN, Choi YJ, Kang DJ, Butler TP, Hasko DG, et al. Nanoscale memory cell based on a nanoelectromechanical switched capacitor. Nature Nanotechnology. 2008;3(1):26-30.
[29] Bean J, Weeks A, Boreman G. Performance optimization of antenna-coupled Al/AlOX/Pt tunnel diode infrared detectors. IEEE J Quantum Electron. 2011;47(1):126-35.
[30] Cowell III EW, Alimardani N, Knutson CC, Conley Jr JF, Keszler DA, Gibbons BJ, et al. Advancing MIM electronics: Amorphous metal electrodes. Adv Mater. 2011;23(1):74-8.
[31] Grossman E, Harvey T, Reintsema C. Controlled barrier modification in Nb/NbOx/Ag metal insulator metal tunnel diodes. J Appl phys. 2002;91(12):10134-9.
[32] Teo K, Lee S, Chhowalla M, Semet V, Binh VT, Groening O, et al. Plasma enhanced chemical vapour deposition carbon nanotubes/nanofibres—how uniform do they grow? Nanotechnology. 2003;14(2):204-11.
[33] Milne W, Teo K, Chhowalla M, Amaratunga G, Lee S, Hasko D, et al. Electrical and field emission investigation of individual carbon nanotubes from plasma enhanced chemical vapour deposition. Diamond and Related Materials. 2003;12(3):422-8.
[34] Teo KB, Minoux E, Hudanski L, Peauger F, Schnell J-P, Gangloff L, et al. Microwave devices: Carbon nanotubes as cold cathodes. Nature. 2005;437(7061):968-.

Supporting Information for

Ultra fast metal-insulator-multi-wall carbon nanotube tunneling diode employing asymmetrical structure effect

Jeong Hee Shin,[1] Jaehan Im, [1] Ji-Woong Choi, [1] Hyun Sik Kim, [2] Jung Inn Sohn, [3]

Seung Nam Cha, [3] and Jae Eun Jang[1,*]

[1]*Department of Information and Communication Engineering, Daegu Gyeongbuk Institute of Science and Technology (DGIST), Daegu, 711-873, Korea*

[2]*Department of Applied Physics and Material Science, California Institute of Technology, Pasadena, CA 91125, U.S.A.*

[3]*University of Oxford, Park Road, Oxford, OX1 3PJ, U. K*

[*]*E-mail: jang1@dgist.ac.kr*

A) Fabrication

A-1) Simple MIM diode

The simple MIM diode was fabricated on Si/SiO_2 (1000 Å) to prevent the devices from unexpected leakage current that leads to low performance. There are three different material combinations, Al-AlO_x-Al, Ni-NiO_x-Ni, and Al-AlO_x-Pt, to investigate the effect of work function difference. All patterns were formed by photolithography and lift-off. Al (4N of purity), Ni (4N5 of purity), and Pt (4N of purity) were deposited by sputtering system. We employ native oxide to form insulator layer. Aluminum and nickel are to easily get thin native oxide, as thin as 56Åm measured in Hitachi HF-3300 TEM, as shown in Fig. S1.

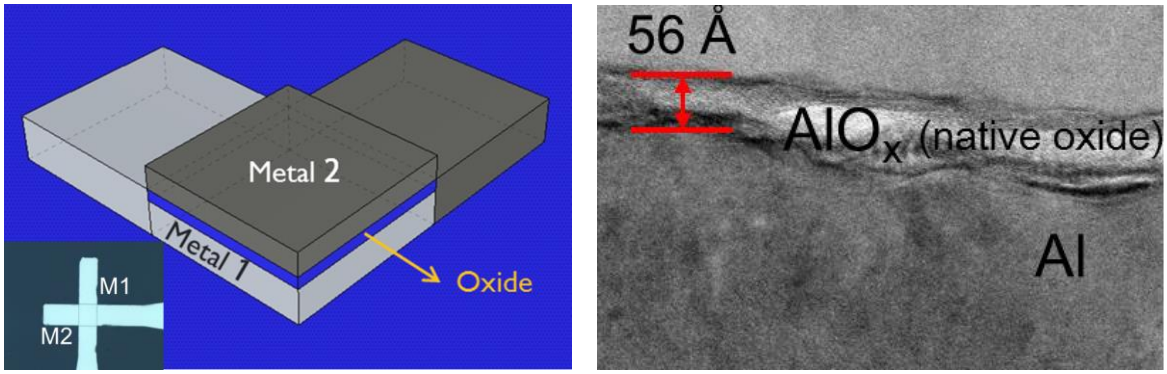

(a) (b)

Fig. S1: Simple MIM diode (a) Schematic diagram and inset fig. is an optical microscope image (b) The TEM image of cross-section view of Al-AlO_x (native oxide layer)

A-2) Lateral MIM diode

The structure of lateral MIM diode is similar with the laid point contact MIM diode. The Si/SiO_2 (1000 Å) is used to block unexpected current from other path ways. The fabrication is composed of photolithography and electron beam lithography (EBL) for pad and sharp tip shape, respectively. It commonly employs PMMA (polymethyl methacrylate) that is very sensitive to high energy electrons for direct write EBL. JEOL JBX-9300FS E-beam lithography was used for a sharp tip. Nb and Pt were used for flat and sharp tip electrode and deposited by sputtering system. SiO_2 layer is also defined by photolithography and sputtering system.

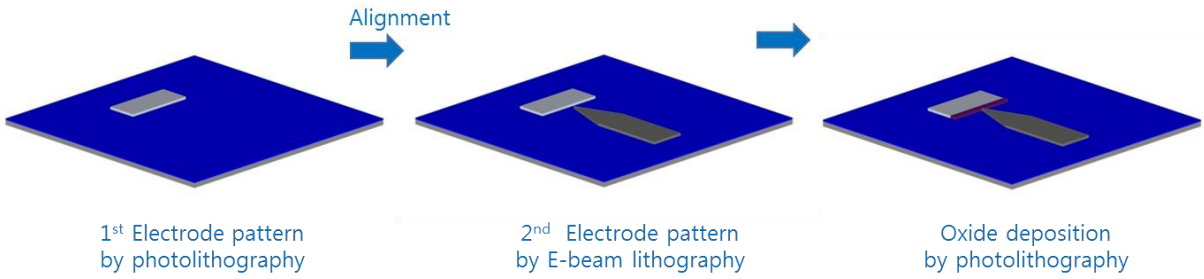

Fig. S2: Fabrication step of Lateral MIM diode

A-3) MIC diode

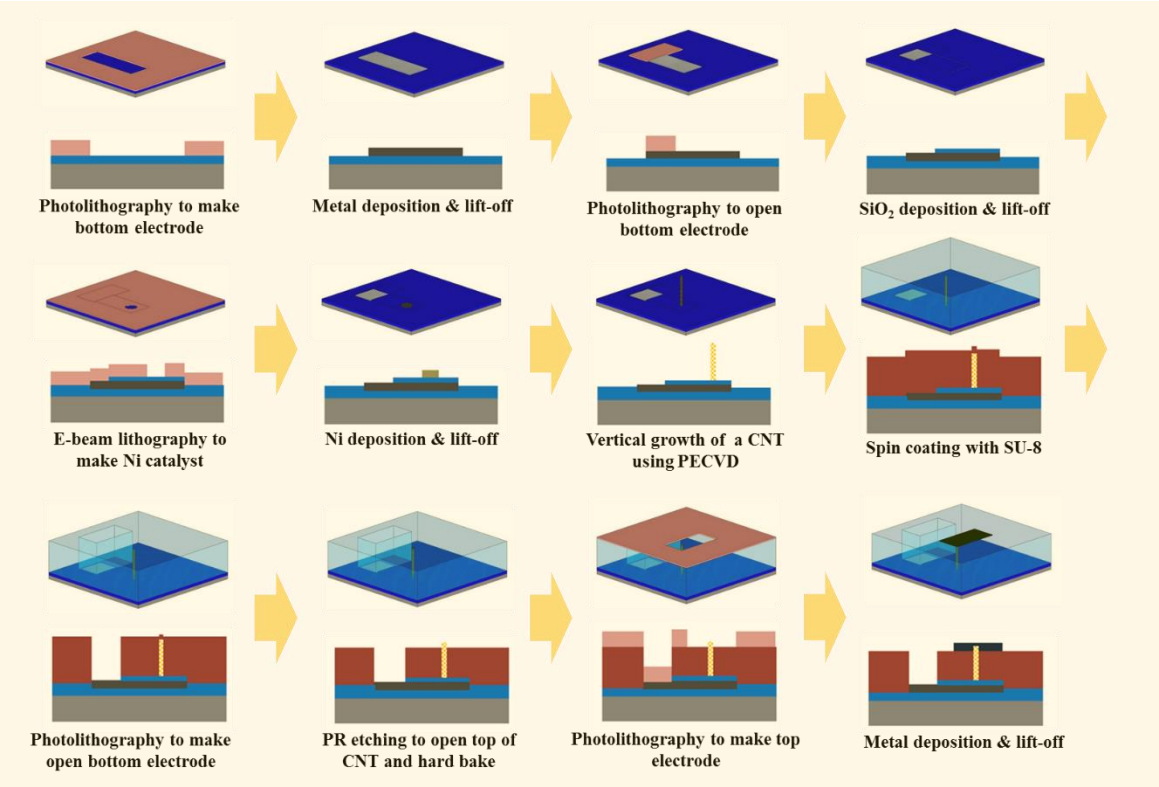

(a)

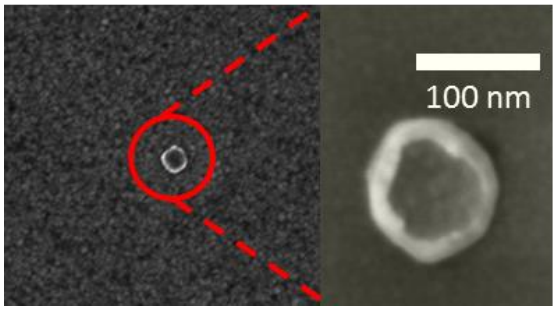

(b)

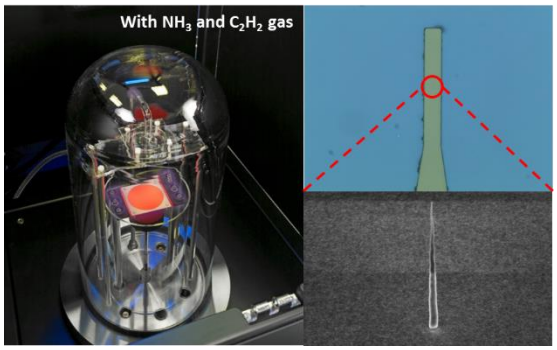

(c)

Fig. S3: Schematic diagram of fabrication step with structure images

(a) Whole fabrication process of MIC diode with 3-dimensional and cross-sectional view; Bottom electrode was formed by photolithography. AZ GXR 601 was coated as 1um thickness and was exposed with 60mJ/cm^2 dose. Sputtering system was used to deposit Nb of 150nm thickness and then lift-off process was carried out with acetone. A cycle of this fabrication based on photolithography and lift-off was repeated to form oxide layer with opening bottom electrode. To make Ni catalyst with diameter of 100nm, E-beam lithography was carried out using JEOL JBX-9300FS with 400 uC/cm^2 dose after PMMA A3 950K, E-beam resist, was coated to make 90nm thickness. Ni deposition (20nm thickness) and lift-off process were performed by thermal evaporator system with deposition ratio of 0.5Å/sec and with acetone, respectively. For growth of a vertical multi-wall carbon nanotube (MWCNT), plasma enhanced chemical vapor deposition by AIXTRON's Black Magic 2 inch system was used with an optimized condition. After pump-out up to 6mbar, the graphite substrate was heated up from room-temperature to 555°C with 50°C/min ramp-up speed. After 55sccm of C_2H_2 was injected into the chamber, it was heated up again from 555°C to 565°C with 200°C/min. After keeping

the state for 60 seconds, plasma of 600V was induced for 5minutes. After growth of a vertical MWCNT on selected area, SU-8 was coated as thick as 2um to sustain the top electrode at the top of a vertical MWCNT. To open the bottom electrode, photolithography was performed with 70mJ/cm^2 dose. After removing SU-8 at the top of MWCNT to be in contact with top electrode, hard bake was carried out with 150°C for 10 minutes (heat-up from room temperature to 150°C for 5minutes and keeping the temperature at 150°C for 5minutes). Final step is forming the top electrode. Photolithography was performed with the condition to form the bottom electrode. Al deposition (approximately 300nm) was sputtered and lift-off process was carried out with acetone.

(b) The SEM image of a Ni catalyst on selected location of bottom electrode (Nb) and its magnified view; size is approximately 100 nm.

(c) Growth of a vertical MWCNT using plasma enhanced chemical vapor deposition (PECVD) by Black Magic 2 inch system (left image). After PECVD process, a MWCNT was grown on the bottom electrode; optical microscope and 45° tilted SEM image (right upper and bottom images, respectively).

B) Experiment for electrical characteristics and rectification performance

Simple MIM diode

Simple MIM diodes can be composed by Al-AlO_x-Al, Ni-NiO_x-Ni, Al-AlO_x-Pt combinations. Table S1 shows work functions of each material, aluminum, nickel, and platinum. Figure S4 illustrates the band diagram of sets of Al-AlO_x-Al, Ni-NiO_x-Ni, Al-AlO_x-Pt. In case of simple MIM diode, the effect of work function difference is important. Thus, we confirm that the how big this effect as function of a diode.

Table S1: Work Functions

Materials	Work functions (eV)
Al	**4.28**
Ni	**5.15**
Pt	**5.65**

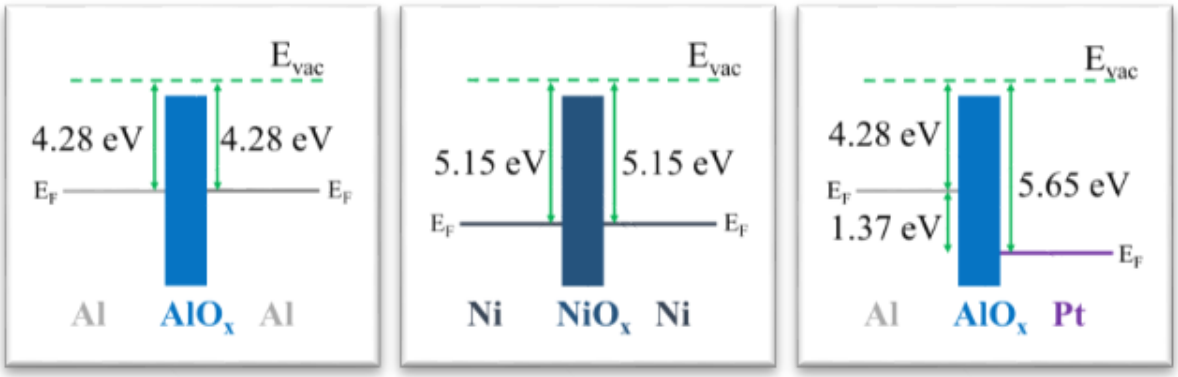

Figure S4: The band diagram of sets of Al-AlO_x-Al, Ni-NiO_x-Ni, Al-AlO_x-Pt

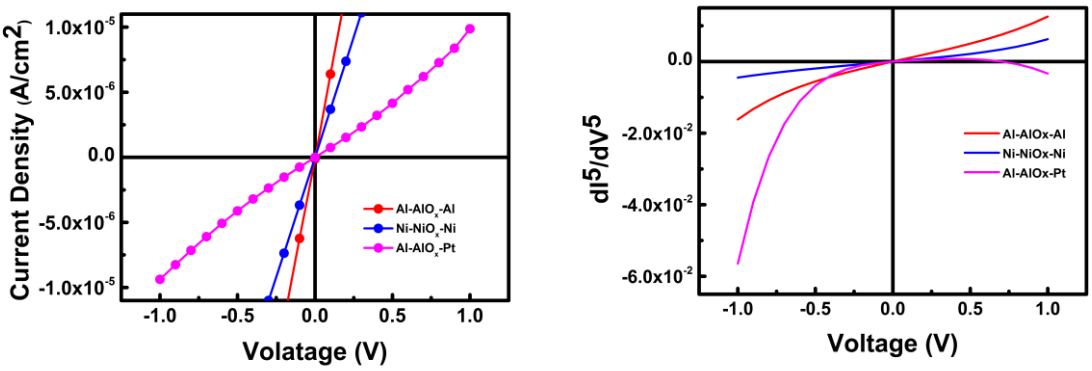

(a) (b)

Figure S5: Electrical characteristics of the simple MIM diode (a) I-V characteristics and (b) fifth-order differentiation of Al-AlO_x-Al, Ni-NiO_x-Ni, Al-AlO_x-Pt.

Figure S4 shows the band diagram of sets of Al-AlO_x-Al, Ni-NiO_x-Ni, Al-AlO_x-Pt. Work function difference of Al-AlO_x-Al and Ni-NiO_x-Ni are 0eV due to same metal in both sides. However, work function difference of Al-AlO_x-Pt is 1.37eV. Al-AlO_x-Al and Ni-NiO_x-Ni devices have the almost symmetrical I-V curve at negative to positive bias sweep, as shown in Figure S5. The work function is related to the energy of the electron, which is associated with the tunneling probability; thus, the probability of tunneling is almost equal to both directions, negative and positive bias, due to the same work function of two electrodes.

Even though Al-AlO_x-Pt structure makes the different barrier formations to the oxide-metal interfaces due to the difference of material work functions, the asymmetric effect of I-V curve is quite small, as shown in Fig. S5. The contrast ratio at ± 1V is about 1.05. Generally the work function difference among metals is below 1eV, so that it is not easy to get high rectifying effect using this MIM structure. The asymmetric phenomenon can be shown at the fifth-order polynomial fit. Since the current can flow to both directions due to the almost symmetric I-V curve, it is hard to expect the rectifying effect despite using the MIM diode

structure. Thus, we conclude that the effect of work function difference is very small for rectification.

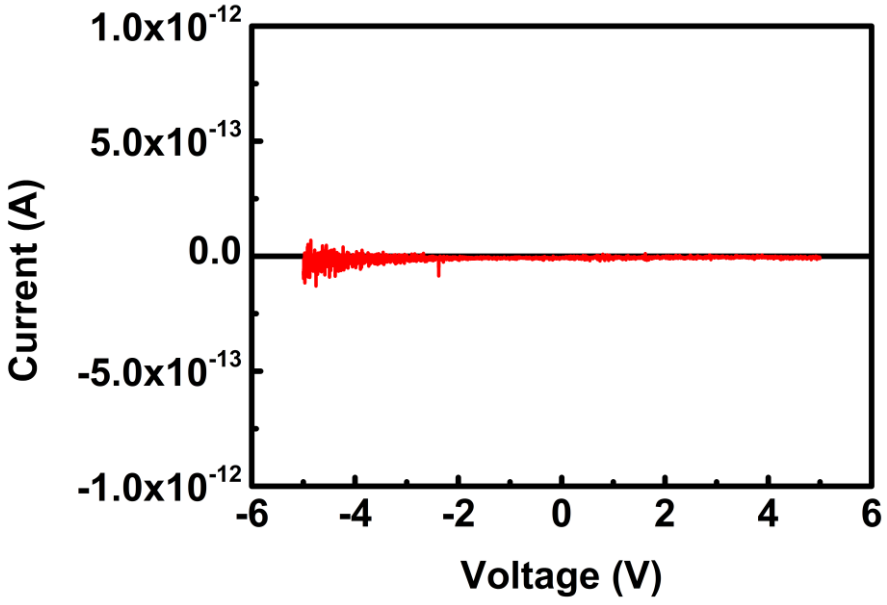

Fig. S6: The graph of leakage current in MIC diode without a vertical CNT

MIC diode without CNT could be fabricated to make sure the current path. In Fig. S3, we skipped only forming Ni catalyst and CNT growth in PECVD. The current level of MIC diode without CNT is about 10^{-13}A. Therefore, we sure that the main current path of MIC diode is CNT through the graph.

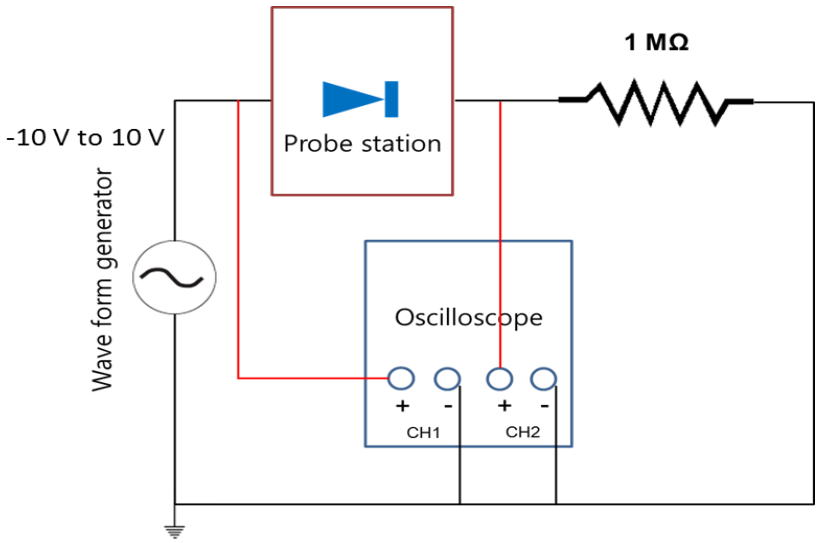

(a)

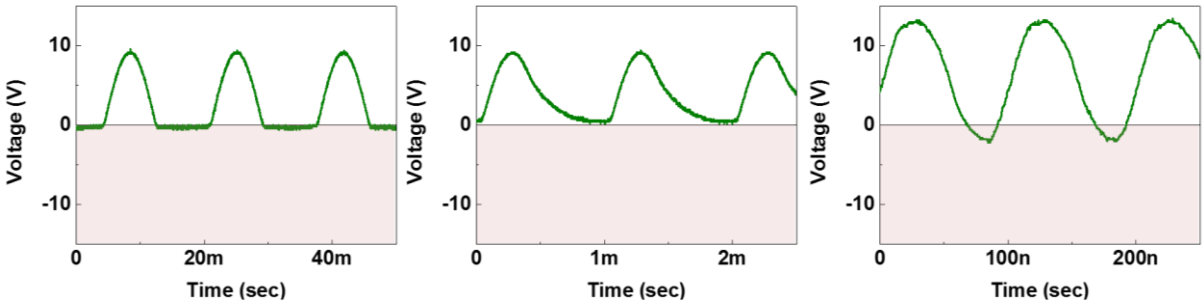

(b)

Fig. S7: (a) Measurement set-up for rectification performance (b) rectifying performance of MIC diode at 60Hz, 1kHz, and 10MHz.

(a) Frequency dependent characteristics have been measured under AC source state by two channel oscilloscope, Tecktronix's TDS 2012C. The AC source was generated by wave form generator, Agilent's 33250A. Dark-shielding probe-station or Au wire bonding was used to connect the sample diodes (but commercial Schottky diode is directly connected without dark-

shielding probe-station) to equipment. To detect the signal amplitude enough, 1MΩ is connected between diode and ground.

(b) MIC structure makes an ideal 'off' state for negative input region at 60Hz. The output signal is identical to the positive input signal area only. With increasing the frequency of input signal to 1KHz, there is still no negative signal, even though the wave shape is changed to a little symmetric form. The parasitic capacitance and the resonance frequency of measurement system can be main reasons for this symmetric effect. At 10MHz input signal, the MIC diode structure recovers the asymmetric signal form with small negative bias.

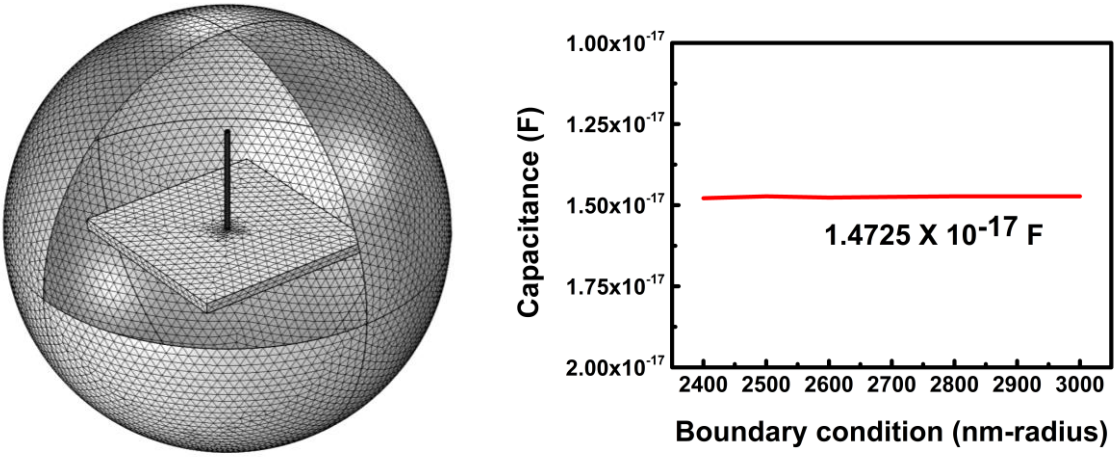

(a) (b)

Fig. S8: (a) Capacitance model in MIC structure from COMSOL (b) simulated capacitance VS boundary condition (radius of sphere) in COMSOL, 14.725 aF.

The capacitance in MIC structure can be obtained by COMSOL. We define the boundary structure as a sphere with various radius. The average capacitance is 14.725 aF.